

Results of the Department of Space Physics, Institute of Atmospheric Physics of the Czech Academy of Sciences, published in 2020

1. First observations of elves and their causative very strong lightning discharges in an unusual small-scale continental spring-time thunderstorm

We showed for the first time that elves can be produced by an unusual small-scale continental spring-time thunderstorm (Fig. 1). The storm occurred in Central Europe, covered a very small area of $\sim 50 \times \sim 30$ km and lasted only for ~ 4 h on April 2, 2017. The fraction of intense positive cloud-to-ground lightning strokes was unusually high, reaching 55%, with a mean peak current of 64 kA. The peak currents of return strokes (RS) associated with elves exceeded ~ 300 kA. Elves and their causative RS were observed with different optical and electromagnetic recordings. Signatures of ionospheric disturbances indicating the presence of elves were found in measurements of displacement currents, ionospheric reflections of sferics and man-made narrow-band transmissions. All these electromagnetic observations coincided with four optical detections of elves and strongly suggest the occurrence of two more elves later in the decaying phase of the storm. Surprisingly, the same electromagnetic measurements indicated that other strong strokes did not produce any elves. Our simulation results showed that the formation of an elve is not only determined by the high-peak current of their causative strokes but that it is also controlled by the conductivity of the lightning channels and velocity of the current wave front. We hypothesized that because of a lower conductivity of RS lightning channels and/or slower current waves only very strong strokes with peak currents above ~ 300 kA might have been capable to produce observable elves during this thunderstorm.



Fig. 1 First observations of elves and their causative very strong lightning discharges in an unusual small-scale continental spring-time thunderstorm.

Reference:

Kolmašová, I., Santolík, O., Kašpar, P., Poppek, M., Pizzuti, A., Spurný, P., et al. (2021). First observations of elves and their causative very strong lightning discharges in an unusual small-scale continental spring-time thunderstorm. *Journal of Geophysical Research: Atmospheres*, 126, e2020JD032825, <https://doi.org/10.1029/2020JD032825>. (Published online: 04 December 2020)

Related references:

Pizzuti, A., J. M. Wilkinson, S. Soula, J. Mlynarczyk, **I. Kolmašová, O. Santolík**, R. Scovell, A. Bennett, M. Füllekrug (2021), Signatures of large peak current lightning strokes during an unusually intense sprite-producing thunderstorm in southern England, *Atmospheric Research*, 249, 105357, <https://doi.org/10.1016/j.atmosres.2020.105357> (Published online: 9 November 2020)

Shklyar, D. R., Manninen, J., Titova, E. E., **Santolík, O., Kolmašová, I.**, & Turunen, T. (2020). Ground and space signatures of VLF noise suppression by whistlers. *Journal of Geophysical Research: Space Physics*, 125, e2019JA027430. <https://doi.org/10.1029/2019JA027430>

Arnone, E., J. Bór, O. Chanrion, V. Barta, S. Dietrich, C.-F. Enell, T. Farges, M. Füllekrug, A. Kero, R. Labanti, A. Mäkelä, K. Mezuman, A. Odzimek, **M. Popek**, M. Prevedelli, M. Ridolfi, S. Soula, D. Valeri, O. van der Velde, Y. Yair, F. Zanotti, P. Zoladek, T. Neubert (2020), Climatology of Transient Luminous Events and Lightning Observed Above Europe and the Mediterranean Sea, *Surveys in Geophysics* 41, 167–199, <https://doi.org/10.1007/s10712-019-09573-5>

2. A model of the subpacket structure of rising tone chorus emissions

The nonlinear growth theory of chorus emissions was used to develop a simple model of the subpacket formation. The model assumes that the resonant current, which is released from the source to the upstream region, radiates a new whistler mode wave with a slightly increased frequency, which triggers a new subpacket. Saturation of the growth in amplitude is controlled by the optimum amplitude. Numerical solution of advection equations for each subpacket, with the chorus equations acting as the boundary conditions, produces a chorus element with a subpacket structure. This element features an upstream shift of the source region with time and an irregular growth of frequency, showing small decreases between adjacent subpackets. The influence of input parameters on the number of subpackets, the shift of the source, the frequency sweep rate, and the maximum amplitude was analyzed. The model well captures basic features of instantaneous frequency measurements provided by the Van Allen Probes spacecraft (Fig. 2). The modeled wave field can be used in future particle acceleration studies.

Reference:

Hanzelka, M., Santolík, O., Omura, Y., **Kolmašová, I.**, & Kletzing, C. A. (2020). A model of the subpacket structure of rising tone chorus emissions. *Journal of Geophysical Research: Space Physics*, 125, e2020JA028094. <https://doi.org/10.1029/2020JA028094>

Related references:

Demekhov, A. G., **Taubenschuss, U., Hanzelka, M., & Santolík, O.** (2020). Frequency dependence of very low frequency chorus Poynting flux in the source region: THEMIS observations and a model. *Geophysical Research Letters*, 47, e2020GL086958. <https://doi.org/10.1029/2020GL086958>

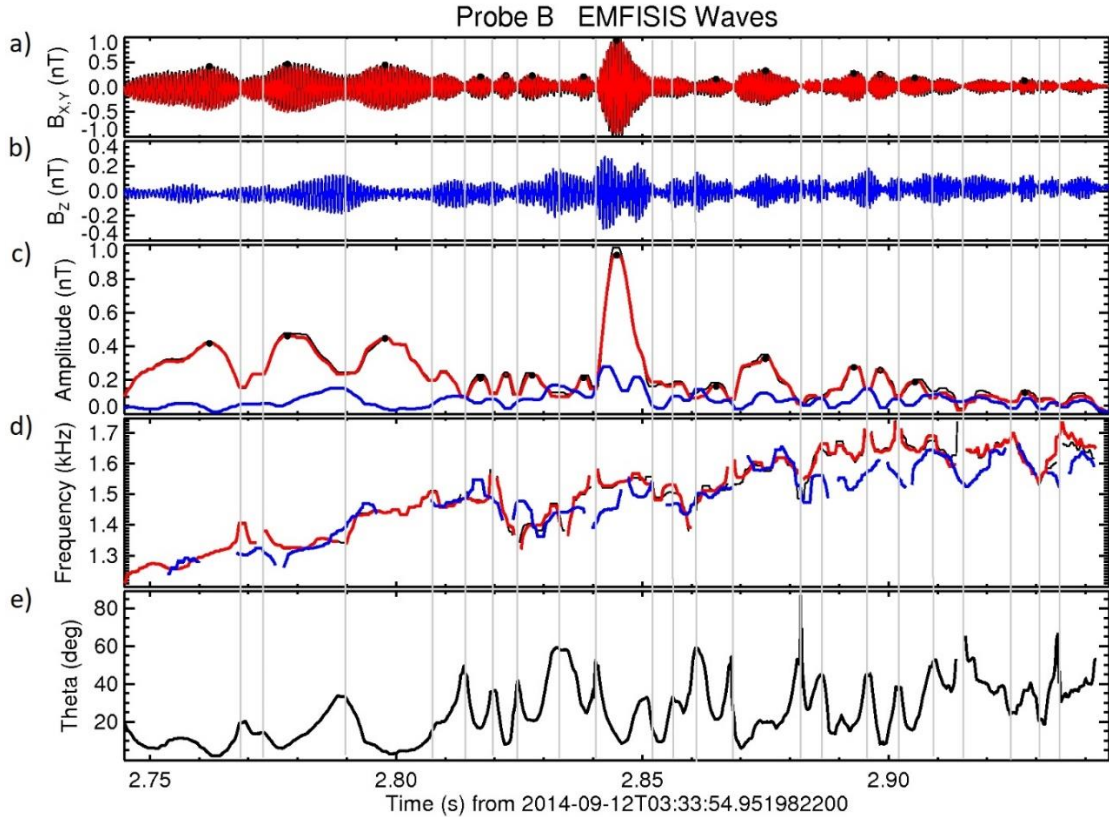


Fig. 2 Detailed analysis of a chorus element recorded by the EMFISIS Waves instrument on Van Allen Probe B on 12 September 2014. (a) Waveform of magnetic field fluctuations perpendicular to the local field line, (b) waveform of the magnetic field fluctuations along the field line, (c) instantaneous amplitudes for the perpendicular and parallel components and for the modulus, shown respectively by red, blue, and black lines, (d) instantaneous frequency with the same color coding plotted for the instantaneous amplitudes larger than 50 pT, (e) instantaneous angle between the wave vector and the local field line; vertical gray lines show the minima of amplitude of the dominant perpendicular component; black dots show its local maxima larger than 50 pT relative to adjacent minima.

3. A multi-instrument approach to determining the source-region extent of EEP-driving EMIC waves

Recent years have seen debate regarding the ability of electromagnetic ion cyclotron (EMIC) waves to drive EEP (energetic electron precipitation) into the Earth's atmosphere. Questions still remain regarding the energies and rates at which these waves are able to interact with electrons. Many studies have attempted to characterize these interactions using simulations; however, these are limited by a lack of precise information regarding the spatial scale size of EMIC activity regions. In this study we examined a fortuitous simultaneous observation of EMIC wave activity by the RBSP-B and Arase satellites in conjunction with ground-based observations of EEP by a subionospheric VLF network (Fig. 3). We described a simple method for determining the longitudinal extent of the EMIC source region based on these observations, calculating a width of 0.75 hr MLT and a drift rate of 0.67 MLT/hr. We described how this maybe applied to other similar EMIC wave events.

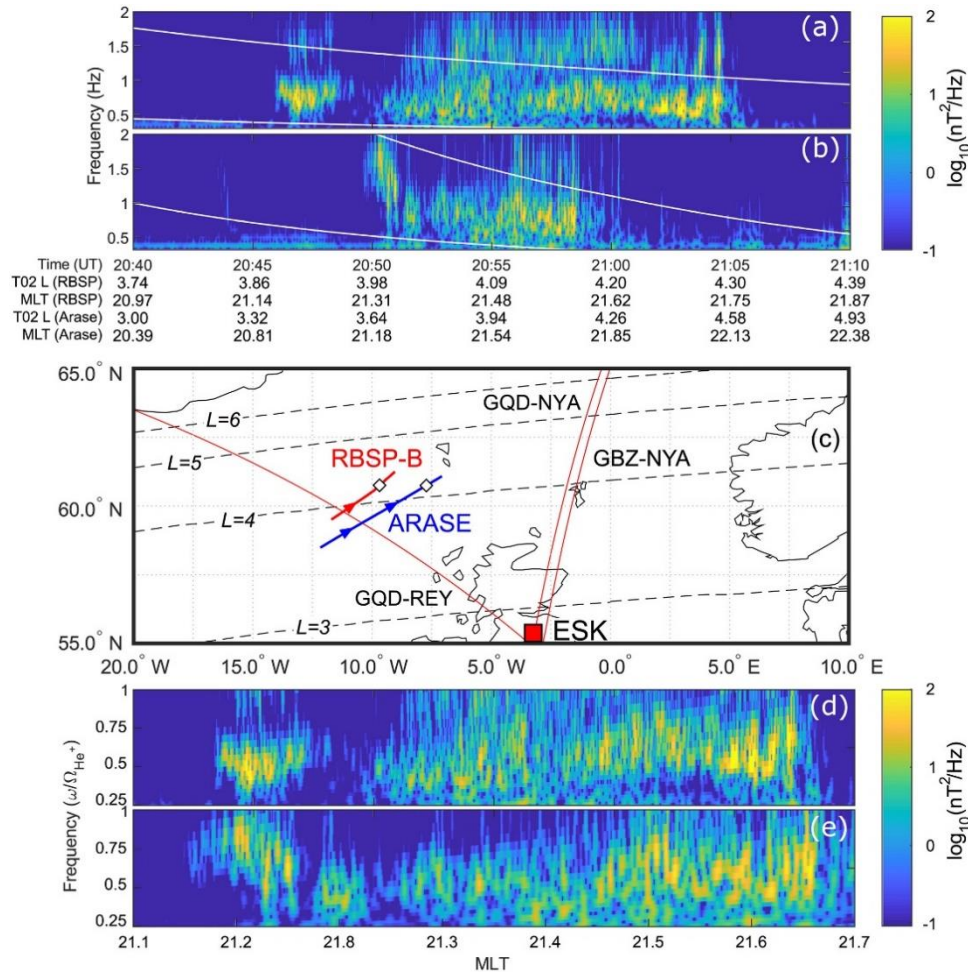


Fig. 3 (a) Wavelet spectrogram of the RBSP-B perpendicular wave power (field-aligned coordinates), with the helium and oxygen gyrofrequencies plotted in white. (b) As in (a) but for the data from the Arase MGF instrument. (c) Map of the event region with the RBSP-B and Arase T02 footprints in red and blue, respectively (with arrows indicating the direction of travel and white diamonds indicating the point of closest approach); the 3 AARDDVARK VLF paths in red; and the Eskdalemuir SCM (red square). T02 Lshells from 3–6 are shown as dashed black lines. (d and e) As in (a) and (b) but plotted against MLT and normalized by the equatorial helium gyrofrequency.

Reference:

Hendry, A. T., Santolik, O., Miyoshi, Y., Matsuoka, A., Rodger, C. J., Clilverd, M. A., et al. (2020). A multi-instrument approach to determining the source-region extent of EEP-driving EMIC waves. *Geophysical Research Letters*, 47, e2019GL086599. <https://doi.org/10.1029/2019GL086599>

4. Whistler mode quasiperiodic emissions: Contrasting Van Allen Probes and DEMETER occurrence rates.

Quasiperiodic emissions are magnetospheric whistler mode waves at frequencies between about 0.5 and 4 kHz which exhibit a nearly periodic time modulation of the wave intensity. We used large data sets of events observed by the Van Allen Probes in the equatorial region at larger radial distances and by the

low-altitude DEMETER spacecraft (Fig. 4). While Van Allen Probes observed the events at all local times and longitudes, DEMETER observations were limited nearly exclusively to the daytime and significantly less frequent at the longitudes of the South Atlantic Anomaly. Further, while the events observed by Van Allen Probes were smoothly distributed over seasons with only mild maxima in spring/autumn, DEMETER occurrence rate had a single pronounced minimum in July. We explained this apparent inconsistency by considering a nondipolar Earth's magnetic field and significant background wave intensities which in these cases prevented the quasiperiodic events from being identified in DEMETER data.

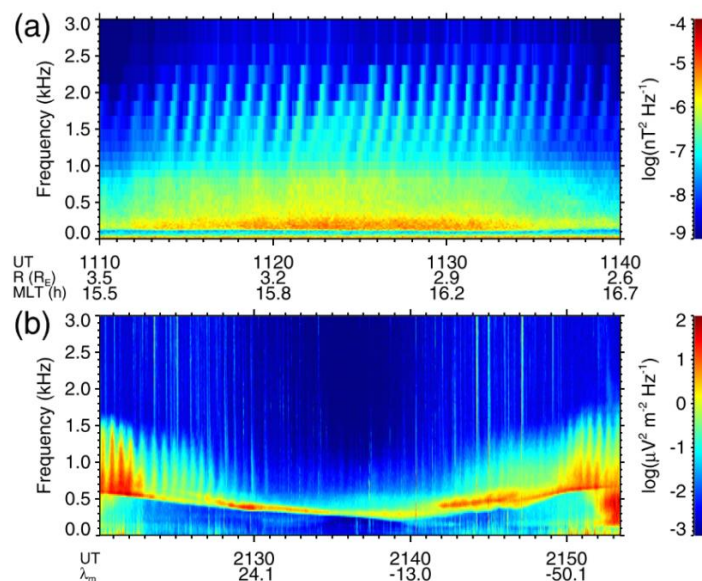


Fig. 4 (a) Frequency-time spectrogram of power spectral density of magnetic field fluctuations measured by the Van Allen Probe A spacecraft on 4 October 2017 close to the equatorial plane. Several quasiperiodically occurring elements at frequencies between about 1 and 2.5 kHz can be identified. (b) Frequency-time spectrogram of power spectral density of electric field fluctuations measured by the DEMETER spacecraft on 13 August 2010 during a daytime half orbit. The spacecraft moved from the north to the south. Quasiperiodically occurring elements at frequencies between about 0.5 and 1.5 kHz can be observed at larger geomagnetic latitudes in both hemispheres, with the intensity fading toward the geomagnetic equator.

Reference:

Nemec, F., Santolík, O., Hospodarsky, G. B., Hajoš, M., Demekhov, A. G., Kurth, W. S., et al. (2020). Whistler mode quasiperiodic emissions: Contrasting Van Allen Probes and DEMETER occurrence rates. *Journal of Geophysical Research: Space Physics*, 125, e2020JA027918. <https://doi.org/10.1029/2020JA027918>

Related references:

Nemec, F., Tomori, A., Santolík, O., Boardsen, S. A., Hospodarsky, G. B., Kurth, W. S., et al. (2020). Fine harmonic structure of equatorial noise with a quasiperiodic modulation. *Journal of Geophysical Research: Space Physics*, 125, e2019JA027509. <https://doi.org/10.1029/2019JA027509>

Martinez-Calderon, C., Němec, F., Katoh, Y., Shiokawa, K., Kletzing, C., Hospodarsky, G., Santolik, O. et al. (2020). Spatial extent of quasiperiodic emissions simultaneously observed by Arase and Van Allen

Probes on 29 November 2018. *Journal of Geophysical Research: Space Physics*, 125, e2020JA028126. <https://doi.org/10.1029/2020JA028126>

Bezdeková, B., Nemec, F., Manninen, J., Hospodarsky, G. B., **Santolík, O.**, Kurth, W. S., & Hartley, D. P. (2020). Conjugate observations of quasiperiodic emissions by the Van Allen Probes spacecraft and ground-based station Kannuslehto. *Journal of Geophysical Research: Space Physics*, 125, e2020JA027793. <https://doi.org/10.1029/2020JA027793>

Demekhov, A. G., Titova, E. E., Manninen, J., Pasmanik, D. L., Lubchich, A. A., **Santolík, O.**, et al. (2020). Localization of the source of quasiperiodic VLF emissions in the magnetosphere by using simultaneous ground and space observations: A case study. *Journal of Geophysical Research: Space Physics*, 125, e2020JA027776. <https://doi.org/10.1029/2020JA027776>

5. Two propagation scenarios of isolated breakdown lightning processes in failed negative cloud-to-ground flashes

Isolated breakdown process (also known as attempted leader or inverted intra-cloud discharge) is a lightning phenomenon characterized by radio wave pulses similar to signatures of preliminary breakdown before negative cloud-to-ground flashes, but in this case no cloud-to-ground return strokes occur. We identified 128 isolated breakdown pulse trains in measurements collected in the Mediterranean by a broadband receiver (0.005–7 MHz) in 2015 and 2018. By combining these records with concurrent Lightning Mapping Array measurements of very high frequency radiation (60–66 MHz) emitted by in-cloud discharges we investigate the development of each discharge (Fig. 5). We identify two scenarios: Either the discharges continue to propagate almost horizontally for more than 150 ms (73%), or they quickly fade out (27%). The geo-localized sources of the observed isolated breakdown pulse trains, together with their waveform characteristics (duration, inter-pulse intervals, regularity, and bipolar shapes) show that both scenarios are similar to initiation processes preceding negative cloud-to-ground flashes.

Reference:

Kolmašová, I., Santolík, O., Defer, E., **Kašpar, P., Kolínská, A.,** Pedebay, S., & Coquillat, S. (2020). Two propagation scenarios of isolated breakdown lightning processes in failed negative cloud-to-ground flashes. *Geophysical Research Letters*, 47, e2020GL090593. <https://doi.org/10.1029/2020GL090593>

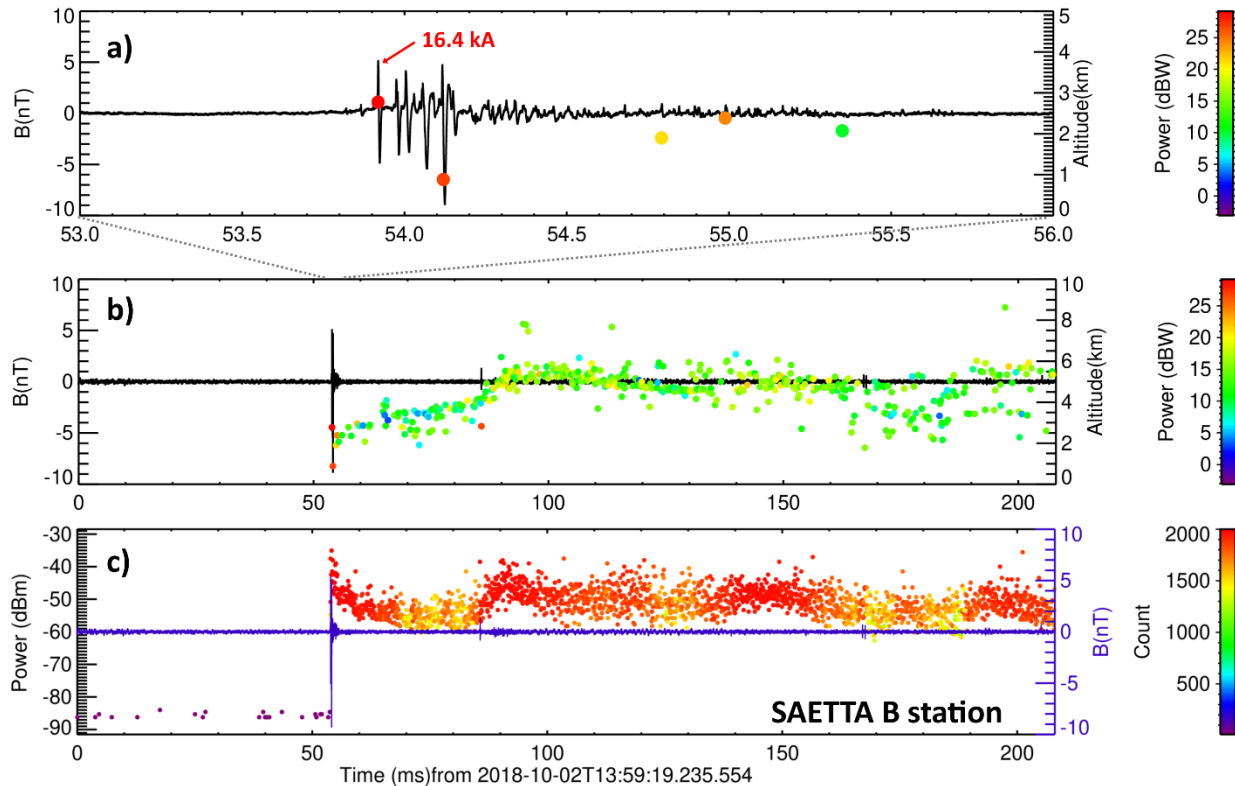


Fig. 5 Example of an isolated breakdown event (Type A) occurring on 2 October 2018 at 13:55:19.236 UT: (a) A 3 ms long detail of the BLESKA waveform showing a sequence of isolated breakdown pulses overlaid on altitude of geo-located SAETTA VHF radiation sources color coded by their power; (b) the whole 208 ms long BLESKA record with geo-located VHF radiation sources; (c) the BLESKA record with peaks of radiated VHF power recorded at the SAETTA Station B (color coded by their counts within individual $80\mu\text{s}$ LMA windows);

6. High-spatiotemporal resolution observations of Jupiter lightning-induced radio pulses associated with sferics and thunderstorms

Jupiter lightning illuminates clouds and produces a strong pulse at radio wavelengths. Juno's radio observatory (consisting of two onboard instruments) in a broad radio range made several detections of extraordinary radio pulses on 6 April 2019. The high-temporal observations of such radio pulses detected below 150 kHz indicate variations of the lightning related processes on the order of submilliseconds. Observations of these radio pulses and direct lightning-induced radio emissions at 600 MHz came from the same area, very close to deep water clouds detected by the Hubble Space Telescope (HST) in the Jovian atmosphere (Fig. 6). The coordinated Juno-HST lightning observations provided a new way of understanding the lightning processes and lightning source regions associated with the cloud features at Jupiter.

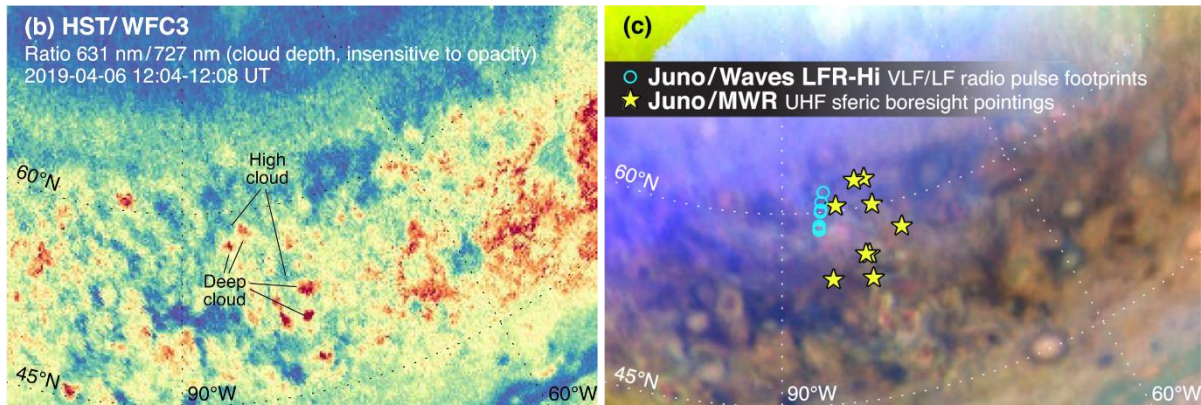


Fig. 6 Polar-projected maps from the Hubble Space Telescope showed that the general source area for Juno lightning events included the three cloud structure elements that are typical of active convection: deep water clouds, high convective towers, and cloud clearings. Color ratio in panel (b) shows cloud depth information (but not opacity information), with high values (red) where clouds are deeper than ~ 4 bar and low values (blue) where opacity is dominated by higher-altitude particulates. Color composites of 631 nm (red channel), 727 nm (green channel), and 889 nm (blue channel) in panel (c) give cloud/haze height information in color and opacity information in brightness. In this composite, deep clouds appear red, high and thick clouds such as convective towers appear white, and clearings appear dark. Tropospheric clearings have a bluish cast at high latitudes because polar stratospheric haze scattering is strong in the 889-nm filter. The magnetic footprints of VLF/LF radio pulses are spatially correlated with nine MWR UHF sferic boresight pointings (blue circles). UHF sferic observations are shown as yellow stars.

Reference:

Imai, M., Wong, M. H., Kolmašová, I., Brown, S. T., Santolík, O., & Kurth, W. S., et al. (2020). High-spatiotemporal resolution observations of Jupiter lightning-induced radio pulses associated with sferics and thunderstorms. *Geophysical Research Letters*, 47, e2020GL088397. <https://doi.org/10.1029/2020GL088397>

Related references:

Sulaiman, A. H., Hospodarsky, G. B., Elliott, S. S., Kurth, W. S., Gurnett, D. A., Imai, M., M. Imai, F., Allegrini, B. Bonfond, G. Clark, J. E. P. Connerney, R. W. Ebert, D. J. Gershman, V. Hue, S. Janser, S. Kotsiaros, C. Paranicas, O. Santolík, J. Saur, J. R. Szalay, S. J. Bolton (2020). Wave-particle interactions associated with Io's auroral footprint: Evidence of Alfvén, ion cyclotron, and whistler modes. *Geophysical Research Letters*, 47, e2020GL088432. <https://doi.org/10.1029/2020GL088432>

Erard, S., Cecconi, B., Le Sidaner, P., Chauvin, C., Rossi, A.P., Minin, M., Capria, T., Ivanovski, S., Schmitt, B., Génot, V., André, N., Marmo, C., Vandaele, A.C., Trompet, L., Scherf, M., Hueso, R., Määttänen, A., Carry, B., Achilleos, N., Soucek, J., Pisa, D., Benson, K., Fernique, P. and Millour, E., 2020. Virtual European Solar & Planetary Access (VESPA): A Planetary Science Virtual Observatory Cornerstone. *Data Science Journal*, 19(1), 22. <http://doi.org/10.5334/dsj-2020-022>

7. Density Fluctuations in the Solar Wind Based on Type III Radio Bursts Observed by Parker Solar Probe

Radio waves are strongly scattered in the solar wind, so that their apparent sources seem to be considerably larger and shifted than the actual ones. Since the scattering depends on the spectrum of density turbulence, a better understanding of the radio wave propagation provides indirect information on the relative density fluctuations at the effective turbulence scale length. Here, we analyzed 30 type III bursts detected by Parker Solar Probe (PSP). For the first time, we retrieved type III burst decay times between 1 and 10 MHz thanks to an unparalleled temporal resolution of PSP. We observed a significant deviation in a power-law slope for frequencies above 1 MHz when compared to previous measurements below 1 MHz by the twin-spacecraft Solar TERrestrial RELations Observatory (STEREO) mission. We noted that altitudes of radio bursts generated at 1 MHz roughly coincide with an expected location of the Alfvén point, where the solar wind becomes super-Alfvénic. By comparing PSP observations and Monte Carlo simulations, we predicted relative density fluctuations at the effective turbulence scale length at radial distances between 2.5 and 14 Solar radii to range from 0.22 to 0.09 (Fig. 7). Finally, we calculated relative density fluctuations measured in situ by PSP at a radial distance from the Sun of 35.7 Solar radii during perihelion #1, and perihelion #2 to be 0.07 and 0.06, respectively. It is in a very good agreement with previous STEREO predictions obtained by remote measurements of radio sources generated at this radial distance.

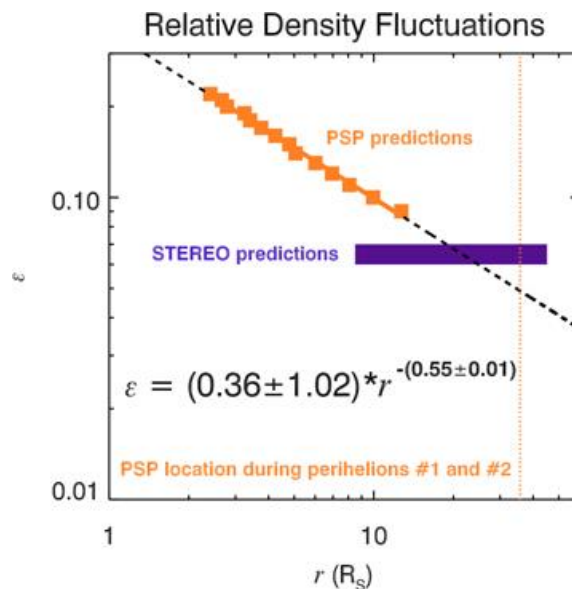


Fig. 7 Results of Monte Carlo simulations and PSP observations. Relative density fluctuations as a function of radial distance are denoted by orange squares. A solid black line represents results of power-law fittings. Predicted relative density fluctuations by STEREO are shown in purple. A dotted orange line indicates the radial distance of PSP during perihelions #1 and #2.

Reference:

Krupar, V. , A. Szabo, M. Maksimovic, **O. Kruparova**, E. P. Kontar, L. A. Balmaceda , X. Bonnin , S. D. Bale et al. (2020), Density Fluctuations in the Solar Wind Based on Type III Radio Bursts Observed by Parker Solar Probe, The Astrophysical Journal Supplement Series 246, 57, <https://doi.org/10.3847/1538-4365/ab65bd>

Related references:

Schmieder, B., Kim, R.-S., **Grison, B.**, Bocchialini, K., Kwon, R.-Y., Poedts, S., & Démoulin, P. (2020). Low Geo-Effectiveness of Fast Halo CMEs Related to the 12 X-Class Flares in 2002. *Journal of Geophysical Research: Space Physics*, 125, e2019JA027529. <https://doi.org/10.1029/2019JA027529>

M. Pick, J. Magdalenic , N. Cornilleau-Wehrin , **B. Grison**, B. Schmieder, and K. Bocchialini, Role of the Coronal Environment in the Formation of Four Shocks Observed without Coronal Mass Ejections at Earth's Lagrangian Point L1 (2020), *The Astrophysical Journal* 895, 144, <https://doi.org/10.3847/1538-4357/ab8fae>

Martinez Oliveros, Juan Carlos; Castillo, Saida Milena Diaz; **Krupar, Vratislav**; Pulupa, Marc; Bale, Stuart D.; Calvo-Mozo, Benjamin (2020), An In Situ Interplanetary "U-burst": Observation and Results, *The Astrophysical Journal* 897, 170, <https://doi.org/10.3847/1538-4357/ab96c3>

Lario, D., R. Y. Kwon, L. Balmaceda, I. G. Richardson , **V. Krupar** , B. J. Thompson , O. C. St Cyr, L. Zhao, and M. Zhang (2020), Fast and Wide CMEs without Observed >20MeV Protons, *The Astrophysical Journal* 889, 92, <https://doi.org/10.3847/1538-4357/ab64e1>

Vandas, M., Nemecek, Z., Safrankova, J., Romashets, E. P., & **Hajoš, M.** (2020). Comparison of observed and modeled magnetic fields in the Earth's magnetosheath. *Journal of Geophysical Research: Space Physics*, 125, e2019JA027705. <https://doi.org/10.1029/2019JA027705>

8. Time Domain Sampler subsystem for the Solar Orbiter mission

Solar Orbiter spacecraft launched successfully in February 2020, carrying (among others) four science instruments dedicated to measuring of the properties of electromagnetic field and plasma at the close vicinity of the spacecraft. These in-situ instruments include a magnetometer MAG, an instrument for detection of velocity distribution function of plasma particles (SWA), energetic particle detector (EPD) and an instrument for measuring radio and plasma waves in the solar wind (RPW). One of the RPW subsystems, the Time Domain Sampler, dedicated to observation of high frequency plasma waves, was developed by the team from the Institute of Atmospheric Physics and members of the Department of space physics are now in charge of its scientific operations, data calibration and processing. The instrument operates nearly continuously since the launch and during this time it returned thousands of waveform measurements of plasma waves and dust particle impacts, including multiple crossings of type III burst source regions (Fig. 8), the first perihelion pass and a flyby of Venus. A special issue of *Astronomy & Astrophysics* published in 2020 brings articles describing the Solar Orbiter instruments, including RPW, and the planning and coordination of the instrument operations on mission level.

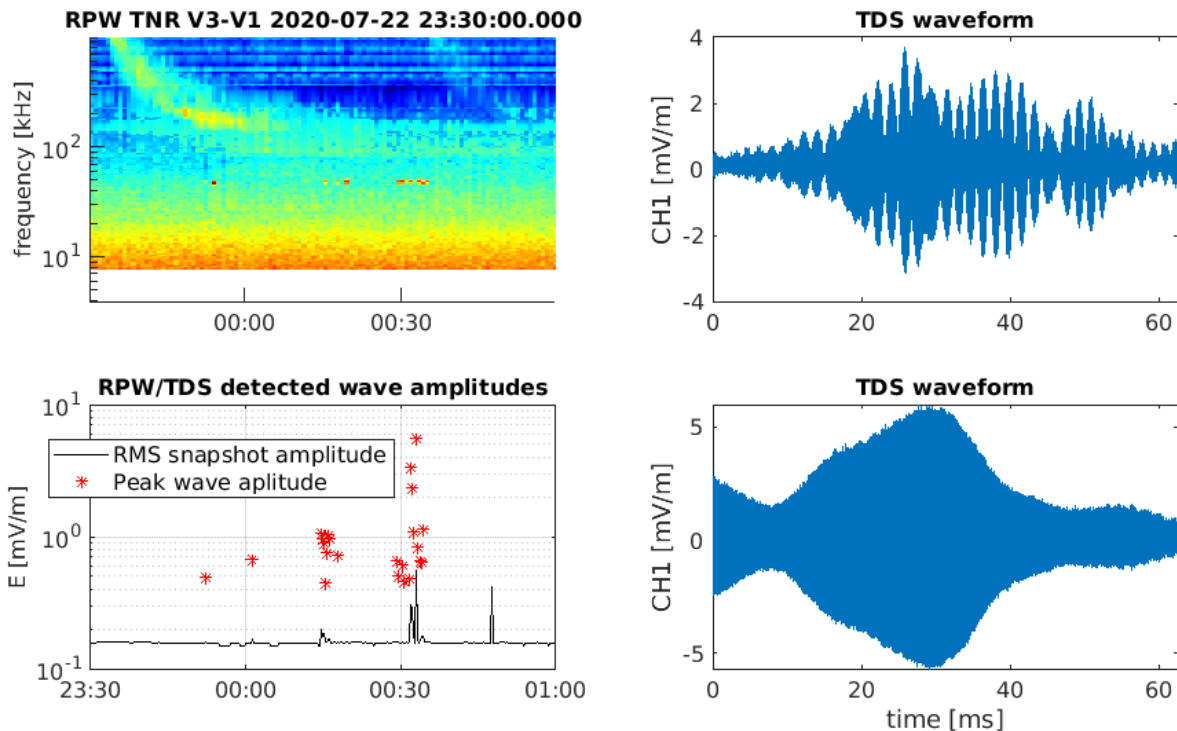


Fig. 8 Type III radio burst observed by Solar Orbiter in July 2020. During this event, Solar Orbiter passed through the source region of the radio emission, where it observed energetic particles and Langmuir waves. In the right half of the figure are shown waveform snapshots of the electric field of Langmuir waves at the electron plasma frequency as measured by RPW-TDS.

Reference:

Maksimovic, M., Bale, S. D., Chust, T., Khotyaintsev, Y., Krasnoselskikh, V., Kretzschmar, M., (...), **Souček, Jan**, Steller, M., Štverák, Štěpán, Trávníček, Pavel, (...), **Santolík, Ondřej, Kolmašová, Ivana, Krupař, Vratislav, Krupařová, Oksana, Piša, David, Uhlíř, Luděk, Lán, Radek**, Baše, Jiří, Ahlen, L., André, M., Bylander, L., Cripps, V., Cully, C., Eriksson, A., Jansson, S.-E., Johansson, E.P.G., Karlsson, T., Puccio, W., Břínek, J., Öttacher, H., Panchenko, M., Berthomier, M., Goetz, K., Hellinger, Petr, (...), 2020: The Solar Orbiter Radio and Plasma Waves (RPW) instrument, *Astronomy & Astrophysics* 624, A12, doi:10.1051/0004-6361/201936214

Related references:

Rodríguez-Pacheco, J., Wimmer-Schweingruber, R.F., Mason, G.M.,... **Souček, J.**,... (2020), The Energetic Particle Detector: Energetic particle instrument suite for the Solar Orbiter mission, *Astronomy & Astrophysics* 642, A7, <https://doi.org/10.1051/0004-6361/201935287>

Zouganelis, I., De Groof, A., Walsh, A. P., ..., **Souček, J.**, Štverák, Š. ,... (2020), The Solar Orbiter Science Activity Plan. Translating solar and heliospheric physics questions into action, *Astronomy & Astrophysics* 642, A3, <https://doi.org/10.1051/0004-6361/202038445>

Walsh, A. P., Horbury, T.S., Maksimovic, M., ..., **Souček, J.**,... (2020), Coordination of the in situ payload of Solar Orbiter, *Astronomy & Astrophysics* 642, A5 <https://doi.org/10.1051/0004-6361/201936894>

Department of Space Physics, Institute of Atmospheric Physics of the Czech Academy of Sciences in 2020

1. Radka Balková, secretary, 50% FTE
2. Zdeněk Griehl, technician, 40% FTE
3. Benjamin Grison, research scientist
4. Michajlo Hajoš, research scientist
5. Miroslav Hanzelka, PhD student, 70% FTE
6. Aaron T. Hendry, postdoctoral associate, *until April 2*
7. Jiří Jánský, research engineer, since May 1
8. Petr Kašpar, postdoctoral associate
9. Ivana Kolmašová, senior research scientist
10. Andrea Kolínská, MSc student, PhD student since October 1, 50% FTE
11. Vratislav Krupař, research scientist, 20%FTE, *on leave since June 8*
12. *Oksana Krupařová, research scientist, on leave*
13. Radek Lán, research engineer
14. Jan Lukačevič, PhD student, 70% FTE
15. David Píša, research scientist
16. Martin Popek, TLE observer, 25% FTE
17. Ondřej Santolík, senior research scientist, head of the department
18. Jan Snížek, research engineer, 50% FTE
19. Jan Souček, senior research scientist, deputy head of the department
20. Hana Špačková, PhD student, 70% FTE
21. Ulrich Taubenschuss, research scientist
22. *Alexander Tomori, PhD student, on leave*
23. Luděk Uhlíř, research engineer
24. Christof Weber, postdoctoral associate, *until January 31*